

# GEOMETRY DEPENDENCE OF CASIMIR FORCES BEYOND THE PROXIMITY APPROXIMATION

THORSTEN EMIG

*Institut für Theoretische Physik, Universität zu Köln, Zùlpicher StraÙe 77,  
D-50937 Köln, Germany*

Casimir interactions between macroscopic objects are strongly influenced by their geometrical features as shape and orientation as well as by their material properties. The effect of geometry is commonly obtained from the proximity approximation (PA). Here we present a path integral quantization for the electromagnetic field in the presence of deformed metallic surfaces. From the resulting effective action the Casimir force between the surfaces can be calculated without the PA. For corrugated surfaces the force is obtained both perturbatively for small deformations and by a numerical approach for general deformation amplitudes. For general dielectric materials with flat surfaces a path integral based derivation of the Lifshitz theory is outlined, pointing towards a possible approach to study the combined effect of deformations and material properties.

## 1 Introduction and Summary

Casimir's seminal prediction of an universal attractive force between two uncharged metallic plates has been confirmed recently in the distance range from 100nm to several micrometer with increasing accuracy in a number of beautiful high precision experiments.<sup>1,2,3,4,5,6,7</sup> High accuracy could be only achieved by a careful inclusion of the corrections to Casimir's ideal result from finite conductivity of the materials, surface roughness and non-zero temperature.<sup>8</sup> Except one,<sup>6</sup> the above cited experiments deviate from the flat-plate geometry in that they use a plane-sphere configuration in order to avoid the difficulty of maintaining a constant plate separation over the entire surface area. The plane-sphere configuration is the standard situation where the proximity (or Derjaguin) approximation (PA)<sup>9</sup> is commonly employed to calculate geometry induced changes of the force. Consider a non-planar surface above a planar surface where their local distance, measured normal to the planar surface, is given by  $H + h(\mathbf{y}_{\parallel})$  with  $\mathbf{y}_{\parallel}$  the 2D in-plane coordinates, i.e.,  $h(\mathbf{y}_{\parallel}) = 0$  corresponds to two parallel flat plates. The PA assumes that the Casimir energy can be computed as the sum of local contributions between *flat* surface elements at their local distance, yielding the total energy per unit surface area

$$\mathcal{E}_{\text{PA}} = \int d^2\mathbf{y}_{\parallel} \mathcal{E}_0[H + h(\mathbf{y}_{\parallel})], \quad (1)$$

where  $\mathcal{E}_0(H) = -(\pi^2/720)(\hbar c/H^3)$  is the Casimir energy per unit area between two plane surfaces. This approximation is ambiguous since one could just as well measure the local distances normal to the curved surface, yielding

a different result. Below, we will discuss this point further when comparing the PA to our perturbative and numerical results. The PA is expected to hold if both the local surface curvature radii are much larger than the local distance and strongly non-parallel surface elements are at larger separations than more parallel ones.<sup>11</sup> A conceptual different approximation is the pairwise summation of renormalized retarded van der Waals forces.<sup>8</sup> For the geometry considered here it yields exactly the PA result of Eq. (1).<sup>10</sup> For the plane-sphere geometry used in experiments, one can set  $h(\mathbf{y}_{\parallel}) = \mathbf{y}_{\parallel}^2/2R$  with radius of curvature  $R$ , yielding the approximate force  $F_{\text{PA}} = 2\pi R\mathcal{E}_0(H)$ . The latter formula is used in experiments, and there it is justified for that  $R$  is much larger than  $H$ .<sup>a</sup>

For more general geometries the collective nature of the Casimir force suggests it to have a non-trivial and unexpected dependence on the shape of the interacting objects. Whereas the van der Waals force between electrically polarizable particles is always attractive, even the sign of the Casimir force is geometry dependent. There is little intuition for the value of the sign as demonstrated by the repulsive force for a thin conducting shell.<sup>12,13</sup> Due to the importance of Casimir forces in many fundamental and applied contexts, it is highly desirable to obtain a better understanding of its strong geometry dependence, including distinctions from pairwise additive interactions and possibly repulsive forces between *disconnected* surfaces. A promising and experimentally testable route to this end is via modifications of the parallel plate geometry.<sup>14</sup> In an experimental search for novel shape dependencies, Mohideen *et al.* measured the force between a sphere and a sinusoidally corrugated plate with a wave length being larger than the studied range of sphere-plate separations.<sup>15</sup> Their results showed clear deviations from the PA prediction. While it has been suggested that lateral forces caused this deviations<sup>16</sup>, our results indicate a much stronger sensitivity to geometry at smaller corrugation wave lengths.

We demonstrate that a path integral quantization of the electromagnetic field subject to appropriate boundary conditions is a powerful method both for perturbative<sup>14,10</sup> and numerical<sup>17</sup> computations of Casimir interactions. While the well-known boundary conditions for ideal metals are local, we derive non-local boundary conditions for general dielectric materials which reproduce the standard Lifshitz theory in the limit of flat surfaces. For the force between deformed surfaces of ideal metals we find the following results. For general uniaxial deformations we obtained the Casimir force perturbatively to second order in the deformation amplitude  $a$ . At this order, significant deviations from the PA result are found if the deformation wavelength  $\lambda$  is of the same order or smaller than the mean surface distance  $H$ . We apply the perturbative results to sinusoidally corrugated surfaces, see Fig. 1(a). The deformation

---

<sup>a</sup>A numerical scalar field analysis yields sizable deviations from the PA for  $R \lesssim 50H$ .<sup>11</sup>

induced change in the force shows for  $\lambda \ll H$  a slower decay  $\sim H^{-5}$  compared to the  $H^{-6}$  behavior from the PA. However, the perturbative approach is limited to the cases where  $a$  is smaller than both  $H$  and  $\lambda$ . This can be understood by comparing the perturbative approach to the multiple scattering approach of Balian and Duplantier<sup>13</sup> which yields the Casimir energy as a sum over waves propagating along closed paths which scatter at an even number of positions on the surfaces. Each path contributes with a geometric factor which measures at each position the scattering direction relative to the local surface normal. For a series of scatterings on the same surface with all scattering directions being almost perpendicular to the surface normal the geometric factor is small. Our perturbative approach allows in principle for paths with an arbitrarily large number of scatterings. However, it corresponds to an expansion of the geometric factor to second order in the surface deformations. This amounts to the restriction to two successive scatterings on one surface before the wave propagates to the other surface and experiences for the rest of its path only scatterings normal to the surface. This expansion is only justified for surface geometries where  $a$  is smaller than  $\lambda$  so that the scattering directions lie nearly in the mean surface plane. The restriction can be bypassed by an exact evaluation of the path integral by an algorithm which was developed for corrugated surfaces.<sup>17</sup> This numerical approach is applied to the rectangular grating of Fig. 1(b). It confirms the crossover of the force change from a decay  $\sim H^{-6}$  to  $\sim H^{-5}$  at  $H \simeq \lambda$ . In the limit of  $\lambda \lesssim a$  strong corrections to the perturbative results are found. For  $\lambda \rightarrow 0$  the force corresponds to that of two planar plates at a reduced distance  $H - a$  and provides an upper bound to the force at fixed  $H$ . For large  $\lambda$  both the perturbative and the numerical results approach the PA prediction. However, we find that corrections to the PA decay slower with increasing  $\lambda/a$  for the profile with edges [Fig.1(b)] as compared to the smooth profile [Fig.1(a)]. For this finding we provide an interpretation in terms of classical ray optics<sup>18</sup>.

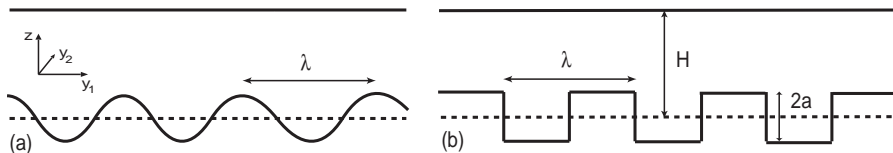


Figure 1. Geometry composed of a flat and a corrugated surface which is studied by perturbation theory (a) and a numerical approach (b). For this two cases the corrections to the proximity approximation scale differently to zero for increasing  $\lambda$ .

## 2 Path Integral Approach

Due to the lack of space we give only a very brief account of the path integral approach<sup>19</sup> and focus instead on explicit results for corrugated surfaces. For the uniaxial geometries considered here, the electromagnetic field can be split into transversal electric (TE) and magnetic (TM) modes which can both be described by a scalar field  $\Phi$ . After a Wick rotation to imaginary time, the field is quantized using the Euclidean action

$$S[\Phi] = \frac{1}{2} \int d^4X (\nabla\Phi)^2. \quad (2)$$

The change in the ground state energy due to the presence of boundaries depends on the type of modes. TM modes are described by Dirichlet boundary conditions,  $\Phi|_S = 0$ , and TE modes correspond to Neumann boundary conditions,  $\partial_{\mathbf{n}}\Phi|_S = 0$ , where  $\partial_{\mathbf{n}}$  is the normal derivative on the surface pointing into the space between the plates. The Casimir interaction between the two surfaces due to TM modes can be obtained from the restricted partition function

$$\mathcal{Z}_{\text{TM}} = \mathcal{Z}_0^{-1} \int \mathcal{D}\Phi \prod_{\alpha=1}^2 \prod_{X_\alpha} \delta[\Phi(X_\alpha)] e^{-S[\Phi]/\hbar}, \quad (3)$$

where  $\mathcal{Z}_0$  is the partition function in the absence of boundaries. For TE modes one obtains  $\mathcal{Z}_{\text{TE}}$  by replacing the argument of the delta-function by  $\partial_{\mathbf{n}}\Phi(X_\alpha)$ . The position of the surfaces are parameterized in the 4D Euclidean space by  $X_1 = [\mathbf{y}, h(\mathbf{y}_{\parallel})]$ ,  $X_2 = [\mathbf{y}, H]$ ,  $\mathbf{y} = (ict \equiv y_0, \mathbf{y}_{\parallel})$ , where  $H$  is their mean distance, and the upper surface is planar. The partition functions can be computed by expanding the delta-functions as  $\prod_{X_\alpha} \delta[\Phi(X_\alpha)] = \int \mathcal{D}\psi_\alpha \exp[i \int_{S_\alpha} dX_\alpha \psi_\alpha \Phi]$  with an auxiliary field  $\psi_\alpha$  defined on each surface. Via the relation  $F = \hbar c / (AL) \partial_H \ln \mathcal{Z}$ , with  $L$  the Euclidean system size in time direction, one finds for the force  $F$  per unit area the result

$$F = -\frac{\hbar c}{2AL} \text{Tr} (M^{-1} \partial_H M). \quad (4)$$

This formula holds separately for both types of modes. For TM and TE modes, respectively, the  $2 \times 2$  matrix kernel read

$$M_{\alpha\beta}^{\text{TM}}(\mathbf{y}, \mathbf{y}') = G[X_\alpha(\mathbf{y}) - X_\beta(\mathbf{y}')] \quad (5a)$$

$$M_{\alpha\beta}^{\text{TE}}(\mathbf{y}, \mathbf{y}') = \partial_{n_\alpha(\mathbf{y}_{\parallel})} \partial_{n_\beta(\mathbf{y}'_{\parallel})} G[X_\alpha(\mathbf{y}) - X_\beta(\mathbf{y}')] \quad (5b)$$

with  $G(\mathbf{y}, z) = (\mathbf{y}^2 + z^2)^{-1}/4\pi^2$  the free Green's function. Below, we will evaluate the force from Eq. (4) both perturbatively in  $h(\mathbf{y}_{\parallel})$  and numerically.

So far we applied the path integral approach only to ideal metal surfaces. If one assumes a splitting into TE and TM modes, arbitrary dielectric surfaces can be described by a path integral with *non-local* boundary conditions for the

scalar field<sup>20</sup>. Planar surfaces with dielectric function  $\epsilon(\omega)$  are described by a mixed boundary condition which reads in momentum  $(k_0, \mathbf{k}_\parallel)$  representation

$$[1 - \Gamma \partial_{\mathbf{n}}] \Phi|_S = 0 \quad (6)$$

with  $\Gamma = [\epsilon(ik_0)k_0^2 + \mathbf{k}_\parallel^2]^{-1/2}$  and  $\Gamma = \epsilon(ik_0)[\epsilon(ik_0)k_0^2 + \mathbf{k}_\parallel^2]^{-1/2}$  for TM and TE modes, respectively. In the limit of ideal metals,  $\epsilon \rightarrow \infty$ , this condition reduces to the above treated Dirichlet and Neumann boundary condition for TM and TE modes, respectively. The condition of Eq. (6) together with the action of Eq. (2) provide a simple derivation<sup>20</sup> of the standard Lifshitz theory.<sup>21</sup> More interestingly, the application of more general non-local boundary conditions to gauge field path integrals might prove useful for studying correlations between geometrical and material dependencies of Casimir forces.

### 3 Perturbative Results

The logarithm of the partition function of Eq. (3) can be expanded in the height profile.<sup>19</sup> With the choice that  $\int d^2\mathbf{y}_\parallel h(\mathbf{y}_\parallel) = 0$  there is no contribution at linear order in  $h(\mathbf{y}_\parallel)$ . At second order the  $H$ -dependent part of  $\ln \mathcal{Z}$  has the form

$$\delta^{(2)} \mathcal{Z} = \frac{\pi^2 L}{240 H^5} \int d^2\mathbf{y}_\parallel h^2(\mathbf{y}_\parallel) - \frac{L}{4} \int d^2\mathbf{y}_\parallel \int d^2\mathbf{y}'_\parallel K(|\mathbf{y}_\parallel - \mathbf{y}'_\parallel|) [h(\mathbf{y}_\parallel) - h(\mathbf{y}'_\parallel)]^2 \quad (7)$$

with a kernel  $K$  which is different for TM and TE modes.<sup>10</sup> From this general result the force for the sinusoidal geometry of Fig. 1(a) can be computed. Assuming  $h(\mathbf{y}_\parallel) = a \cos(2\pi y_1/\lambda)$ , the total force from TM and TE modes assumes the form

$$F = F_{\text{flat}} \left[ 1 + G \left( \frac{H}{\lambda} \right) \left( \frac{a}{H} \right)^2 + \mathcal{O}(a^3) \right] \quad (8)$$

with  $F_{\text{flat}} = -(\pi^2/240)\hbar c/H^4$  the force per unit area between two flat plates. Although the full form of the function  $G(H/\lambda)$  is available<sup>14,10</sup>, we focus here on two limiting cases. For small and large corrugation lengths  $\lambda$ , one finds

$$F/F_{\text{flat}} = 1 + \frac{8\pi}{3} \frac{a^2}{\lambda H} \text{ for } \lambda \ll H, \quad F/F_{\text{flat}} = 1 + 5 \frac{a^2}{H^2} \text{ for } \lambda \gg H. \quad (9)$$

Therefore, for small  $\lambda$  the change of the force decays only like  $H^{-1}$  as compared to  $\sim H^{-2}$  in the previously known limit of large  $\lambda$  for which the PA is expected to hold. The divergence for small  $\lambda$  is an artifact of the perturbative approach as we will show below. Next we compare these results to the predictions of the PA. Depending on which surface this approximation is based, one obtains from Eq. (1) to second order in  $a$  for the force

$$F_{\text{PA,flat}}/F_{\text{flat}} = 1 + 5 \frac{a^2}{H^2}, \quad F_{\text{PA,corr}}/F_{\text{flat}} = 1 + 5 \frac{a^2}{H^2} - 3\pi^2 \frac{a^2}{\lambda^2} \quad (10)$$

for the flat and corrugated plate based PA, respectively. As expected, the later result is smaller due to the increased surface separations when measured normal to the corrugated plate. For  $\lambda \rightarrow \infty$  both results coincide and agree also with the perturbative finding. It is instructive to study how the difference between the full perturbative result of Eq. (8) and the PA decays to zero at large  $\lambda$ . For this difference we find the following expressions which have opposite sign,

$$\frac{F - F_{\text{PA,flat}}}{F_{\text{flat}}} = \left( \frac{4\pi^2}{3} - 20 \right) \frac{a^2}{\lambda^2}, \quad \frac{F - F_{\text{PA,corr}}}{F_{\text{flat}}} = \left( \frac{13\pi^2}{3} - 20 \right) \frac{a^2}{\lambda^2}. \quad (11)$$

Thus, the flat surface based PA overestimates the force while the corrugated surface based PA yields a force which is too small. This underlines the ambiguity of the PA, even for large  $\lambda$  or small surface curvature. Similar observations have been made for a sphere-plane geometry.<sup>11</sup> However, even the exponent of  $a/\lambda$  can depend on details of the corrugated surface. As we will show below, for the rectangular corrugation of Fig. 1(b) the decay towards the PA result is slower as for the present geometry. In the next section we provide an explanation of this strong geometry sensitivity in terms of geometric optics.

#### 4 Exact Numerical Results

We have seen that the perturbative approach is limited to smooth surface profiles where the deformation amplitude  $a$  sets the smallest of the geometrical length scales. The condition for the applicability of perturbation theory is that two arbitrary points on the deformed surface are connected by a vector which is nearly parallel to the reference plane. This is certainly not true for the profile of Fig. 1(a) if  $\lambda \ll a$  but is more generally violated if the profile has vertical segments as it is the case for the rectangular corrugation of Fig. 1(b). For the latter profile, the perturbative expression of Eq. (7) indeed diverges. However, the general result of the path integral approach, Eq. (4), can be used for a precise numerical computation of the force even in cases where perturbation theory fails. For periodic profiles one can apply the following approach.<sup>17</sup> First, the Fourier transformed kernel  $M(\mathbf{y}, \mathbf{y}')$  of Eq. (5) is decomposed into contributions from momenta which are integer multiples of  $2\pi/\lambda$ , i.e.,

$$M(\mathbf{p}, \mathbf{q}) = \sum_{m=-\infty}^{\infty} N_m(p_{\perp}, p_1) (2\pi)^3 \delta(\mathbf{p}_{\perp} + \mathbf{q}_{\perp}) \delta(p_1 + q_1 + 2\pi m/\lambda) \quad (12)$$

with  $\mathbf{p}_{\perp} = (p_0, p_2)$ . The  $2 \times 2$  matrices  $N_m$  are completely determined by a given uniaxial surface profile  $h(y_1)$ . Using Eq. (4), the force per unit area can be then obtained from

$$F = -\frac{\hbar c}{4\pi^2} \int_0^{\infty} dp_{\perp} p_{\perp} \int_0^{\pi/\lambda} dp_1 g(p_{\perp}, p_1), \quad (13)$$

with

$$g(p_{\perp}, p_1) = \text{tr} \left( B^{-1}(p_{\perp}, p_1) \partial_H B(p_{\perp}, p_1) \right), \quad (14)$$

where the lower case symbol  $\text{tr}$  denotes a partial trace with respect to the discrete indices  $k, l$ , and the matrix  $B$  is given by  $B_{kl}(p_{\perp}, p_1) = N_{k-l}(p_{\perp}, p_1 + 2\pi l/\lambda)$  with the  $N_m$  defined by Eq. (12). In the following, we will apply this formula to the profile of Fig. 1(b) for which the matrices  $N_m$  can be obtained analytically.<sup>17</sup>

For  $\lambda \rightarrow 0$ , i.e., if  $\lambda$  is the smallest length scale, the function  $g(p_{\perp}, p_1)$  can be calculated analytically, leading to  $g(p_{\perp}, p_1) = 2p/(e^{2p(H-a)} - 1)$  for both TM and TE modes. After insertion into Eq. (13), one finds the simple result

$$F_0 = -\frac{\pi^2}{480} \frac{\hbar c}{(H-a)^4}. \quad (15)$$

for the force from TM or TE modes, respectively. This result can be obviously interpreted as the force between two planar plates at a reduced distance  $H-a$  which reflects that the relevant modes do not "feel" the narrow valleys of the profile in the limit  $\lambda \ll a, H-a$ . In the opposite limit of very large  $\lambda$ , the PA should be reliable, with the result

$$F_{\text{PA}} = -\frac{\pi^2}{480} \frac{\hbar c}{2} \left( \frac{1}{(H+a)^4} + \frac{1}{(H-a)^4} \right), \quad (16)$$

for both TM and TE modes. Here the PA yields the same result for the flat and the corrugated surface based approximation.

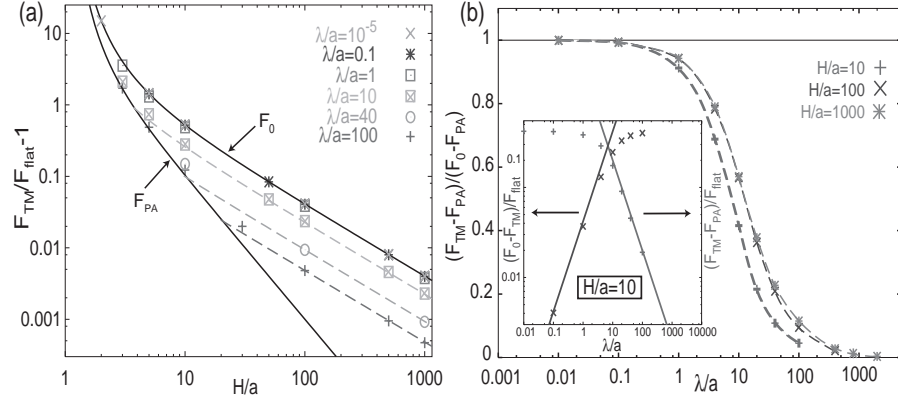


Figure 2. Casimir force  $F_{\text{TM}}$  from TM modes for the geometry of Fig. 1(b). (a) Relative change compared to the force between two flat plates for different corrugation lengths  $\lambda$ . (b) Crossover between the proximity approximation at large  $\lambda$  [Eq. (16)] and the reduced distance result of Eq. (15) at small  $\lambda$ .

For all intermediate values of  $\lambda$ , the force can be calculated numerically from Eq. (13) by defining the  $M$ -th order approximation  $g_M(p_\perp, p_\parallel)$  to the function  $g(p_\perp, p_\parallel)$  by truncating the matrix  $B_{kl}$  symmetrically around  $(k, l) = (0, 0)$  at order  $M$  so that the trace in Eq. (14) extends only over  $k, l = -(M-1)/2, \dots, (M-1)/2$ . This in turn, by numerical integration of Eq. (13), yields a series of forces which can be extrapolated to the actual force at  $M \rightarrow \infty$ . The results for TM modes have been obtained in Ref. <sup>17</sup> and are shown in Fig. 2. The force  $F_{\text{TM}}$  at fixed  $H/a$  is found to be monotonous in  $\lambda/a$  and its minimal value is given by the PA result  $F_{\text{PA}}$  of Eq. (16). At small  $\lambda/a$  the exact result of Eq. (15) is recovered, and the divergence seen in perturbation theory, Eq. (9), is removed. However, in agreement with perturbation theory for the sinusoidal profile, the relative change  $F_{\text{TM}}/F_{\text{flat}} - 1$  of the force shows a crossover at  $\lambda \simeq H$  from a  $H^{-2}$  decay at  $H \lesssim \lambda$  to a  $H^{-1}$  decay at larger  $H$ . Fig. 2(b) shows how the limits of Eqs. (15), (16) are approached with decreasing or increasing  $\lambda$  at fixed  $H/a$ . In the range of studied values for  $H/a$  the crossover between the two limits appears at  $\lambda/a$  of order 10. As shown by the inset of Fig. 2(b) for  $H/a = 10$ , we find that the corrections to the results of Eqs. (15), (16) obey power laws,

$$\frac{F_0 - F_{\text{TM}}}{F_{\text{flat}}} \sim \frac{\lambda}{a}, \quad \frac{F_{\text{TM}} - F_{\text{PA}}}{F_{\text{flat}}} \sim \frac{a}{\lambda} \quad (17)$$

for  $\lambda/a \ll 1$  and  $\lambda/a \gg 1$ , respectively. For TE modes we expect in the first case a decay  $\sim (\lambda/a)^{1/2}$  while in the latter case the exponent will be the same as for TM modes. Comparing to Eq. (11) we observe that the PA limit is approached with a different exponent for large  $\lambda$ . This scaling behavior can be understood from classical ray optics. Following a recently proposed "optimal" PA for a scalar field<sup>18</sup>, the Casimir energy is not obtained from the normal distance based on one of the surfaces [cf. Eq. (1)] but from the *shortest* surface-to-surface ray (of length  $\ell(\mathbf{y}_\parallel, z)$ ) through given positions  $(\mathbf{y}_\parallel, z)$  between the two surfaces of area  $A$ ,

$$\mathcal{E}_{\text{opt}}/\mathcal{E}_0 = \int d^2\mathbf{y}_\parallel \int_{h(\mathbf{y}_\parallel)}^H dz \frac{H^3}{A \ell^4(\mathbf{y}_\parallel, z)}. \quad (18)$$

Of course, this is still an approximation even for small surface curvature since the surfaces are treated as locally flat. However, we expect that this approximation yields the correct scaling behavior for large  $\lambda/a$ . For the rectangular corrugation the lengths of the shortest paths can be computed analytically. For small  $a/H$  the dominant deviation from the standard PA comes from rays through positions located in equal sectors of almost triangular cross section for which the rays end exactly on the upper edges of the corrugated profile. For large  $\lambda$  the volume of a sector becomes *independent* of  $\lambda$ . In this case, a simple calculation yields, using Eq. (18), the correction to the PA force,  $(F_{\text{opt}} - F_{\text{PA}})/F_{\text{flat}} = \frac{112}{9} \sqrt{a/H} a/\lambda$ , which reproduces our numerically



observed decay  $\sim a/\lambda$  of Eq. (17). How can this be reconciled with our perturbative result of Eq. (11) for the sinusoidal profile? The crucial point is that the latter profile has a finite slope across the entire surface. Thus, the shortest length  $\ell$  deviates for *all* positions between the surfaces from the distance used in the standard PA. Using Eq. (18), a model calculation for a corrugation with a piecewise constant slope indeed reproduces a decay  $\sim (a/\lambda)^2$  of the correction to the standard PA result.

So far, we presented numerical results for TM modes only. For TE modes the same approach can be applied to the matrix of Eq. (5). The full electrodynamic Casimir force is then obtained as  $F_{\text{TM}} + F_{\text{TE}}$ . Instead of presenting the results for TE modes independently, it is more useful to look at their relative contribution compared to TM modes. Fig. 3 displays the ratio  $F_{\text{TM}}/F_{\text{TE}}$  of the force from TM and TE modes for different corrugation lengths. Since the force is again bounded from below by  $F_{\text{PA}}$  and from above by  $F_0$ , one has  $F_{\text{TM}}/F_{\text{TE}} \rightarrow 1$  for both  $\lambda/a \rightarrow \infty$  and  $\lambda/a \rightarrow 0$ . However, for intermediate corrugation lengths the ratio can differ from one, with the amount depending on the mean surface distance  $H$ . We observe the tendency that TM mode contributions dominate at smaller  $\lambda$  while for larger  $\lambda$  the TE modes provide a larger force. In contrast, for a sinusoidal profile the force from TM modes is larger at all  $\lambda$ , at least to second order in  $a$ . For very small separations  $H \gtrsim a$  the segments of the rectangular corrugation which are closer to the flat surface yield the main contribution and the PA is expected to hold, implying  $F_{\text{TM}}/F_{\text{TE}} \approx 1$  which indeed can be observed in Fig. 3. In the opposite case of large  $H \gg a$ , one obtains the flat plate geometry, and again  $F_{\text{TM}}/F_{\text{TE}} \rightarrow 1$ . The latter limit is approached for both types of corrugations with a power law  $\sim (H/a)^{-1}$  which we find in perturbation theory as well as in the numerical approach.

## Acknowledgments

I thank B. Duplantier for useful discussions and R. Golestanian, A. Hanke and M. Kardar for their collaboration on part of the work presented here. This project is supported by the Deutsche Forschungsgemeinschaft (DFG) through an Emmy Noether grant.

## References

1. S. K. Lamoreaux, *Phys. Rev. Lett.* **78**, 5 (1997); *Phys. Rev. Lett.* **81**, 5475 (1998); *Phys. Rev. Lett.* **84**, 5673 (2000).
2. U. Mohideen and A. Roy, *Phys. Rev. Lett.* **81**, 4549 (1998).
3. A. Lambrecht and S. Reynaud, *Phys. Rev. Lett.* **84**, 5672 (2000).
4. T. Ederth, *Phys. Rev. A* **62**, 062104 (2000).
5. H. B. Chan *et al*, *Science* **291**, 1941 (2001); *Phys. Rev. Lett.* **87**, 211801 (2001).

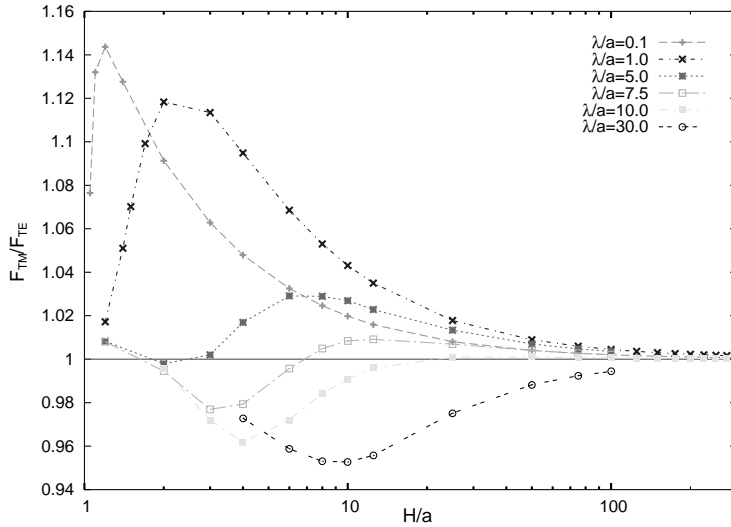


Figure 3. Ratio of the Casimir force from TM and TE modes, respectively, for the geometry of Fig. 1(b).

6. G. Bressi, G. Carugno, R. Onofrio, and G. Ruoso, *Phys. Rev. Lett.* **88**, 041804 (2002).
7. R. S. Decca, D. Lopez, E. Fischbach, and D. E. Krause, *Phys. Rev. Lett.* **91**, 050402 (2003).
8. M. Bordag, U. Mohideen, and V. M. Mostepanenko, *Phys. Rep.* **353**, 1 (2001).
9. B. Derjaguin, *Kolloid-Z.* **69**, 155 (1934).
10. T. Emig, A. Hanke, R. Golestanian, and M. Kardar, *Phys. Rev. A* **67**, 022114 (2003).
11. H. Gies, K. Langfeld, and L. Moyaerts, *JEHP* **06**, 018 (2003).
12. T. Boyer, *Phys. Rev. A* **9**, 2078 (1974).
13. R. Balian and B. Duplantier, *Ann. Phys. (N.Y.)* **112**, 165 (1978).
14. T. Emig, A. Hanke, R. Golestanian, and M. Kardar, *Phys. Rev. Lett.* **87**, 260402 (2001).
15. A. Roy and U. Mohideen, *Phys. Rev. Lett.* **82**, 4380 (1999).
16. G. L. Klimchitskaya, S. I. Zhanette, and A. O. Caride, *Phys. Rev. A* **63**, 14101 (2000).
17. T. Emig, *Europhys. Lett.* **62**, 466 (2003).
18. R. L. Jaffe and A. Scardicchio, preprint quant-ph/0310194.
19. H. Li and M. Kardar, *Phys. Rev. Lett.* **67**, 3275 (1991), R. Golestanian and M. Kardar, *Phys. Rev. Lett.* **78**, 3421 (1997).
20. R. Büscher and T. Emig, preprint cond-mat/0308412.

21. E. M. Lifshitz, *Sov. Phys. JETP* **2**, 73 (1956).